Rapid Communications

Avalanche statistics and the intermittent-to-smooth transition in microplasticity

G. Sparks,[1] Y. Cui,[2] G. Po,[3] Q. Rizzardi,[1] J. Marian,[3,4] and R. Maaß[1,*]

[1]*Department of Materials Science and Engineering and Frederick Seitz Materials Research Laboratory, University of Illinois at Urbana-Champaign, Urbana, Illinois 61801, USA*

[2]*School of Aerospace Engineering, Tsinghua University, Beijing 100084, China*

[3]*Department of Mechanical and Aerospace Engineering, University of California, Los Angeles, Los Angeles, California 90095, USA*

[4]*Department of Materials Science and Engineering, University of California, Los Angeles, Los Angeles, California 90095, USA*

(Received 1 March 2019; published 22 August 2019)

Plastic flow at small scales is generally observed to be intermittent, whereas the stress-strain behavior of bulk crystals is mostly smooth. Here we find that when the external deformation rate of small-scale crystals approaches the speed of the crystallographic slip velocity, an intermittent-to-smooth transition of plastic flow is observed. By defining a rate-dependent intermittency parameter, this phenomenon can be captured with a power law covering 5.5 orders of magnitude for Au and Nb micron-sized single crystals with experiments and via simulations for Nb crystals. Our results indicate that the transition to smooth flow is driven by a gradual truncation of the underlying truncated power law that describes the intermittently evolving system. This is caused by a competition of internal and external rates, which aligns with the well-known transitions from serrated to nonserrated flow in metallic glasses or materials with dynamic strain aging.

DOI: 10.1103/PhysRevMaterials.3.080601

Despite very early experimental evidence of discrete plastic flow of metallic crystals [1,2], plasticity has for many decades been treated as homogenous. Since stress-strain curves of macroscopic crystals are mostly smooth, such an approach seemed justifiable and has resulted in numerous phenomenological flow models that rely on some averaged quantities. Exceptions to the rule of smooth flow are the well-known Portevin–Le Chatelier (PLC) [3–5] effect in solid-solution strengthened crystals, strain localization in metallic glasses [6], or the observation of acoustic emission (AE) pulses recorded from deforming pure single crystals [7,8]. More recent AE experiments have paid close attention to the intermittent appearance of plastic bursts that are characterized by a power-law scaling, suggesting that plasticity may be free of a well-defined scale (average) [9–11]. The fact that intermittency can be detected in AE signals of pure single crystals suggests that dislocations moving collectively in bundles, resulting in so-called *avalanches*, may be the norm rather than the exception.

Another pathway to directly probe fluctuations in stress and strain is to reduce the sample size. Below some dimension, virtually all stress-strain curves from metallic single crystals become intermittent [12], supporting the notion that plastic flow is not a smooth process. Previous investigations on the intermittent stress-strain behavior of small-scale crystals have focused on the scale-free behavior of displacement jump-size distributions [13–17]. These studies report pure or truncated power-law behavior that, via similar scaling exponents, suggest a fundamental universal aspect of plasticity shared by many different materials, which makes intermittent flow material-nonspecific. This is interesting from a general physics perspective, but from a materials physics viewpoint it is the differences between materials that allow explaining their specific behavior. Indeed, very recent work shows that scaling exponents of microplasticity are nontrivial, which applies both to the event sizes and the spatiotemporal avalanche dynamics [18–21].

Another fundamental and intriguing aspect that emanates from such experiments is that, in addition to the material-dependent response, there is a testing device-dependent effect on the measured slip velocities [18,22,23]. As previous studies show [19,24–26], the most important variable is the externally applied deformation rate, suggesting that—within the data scatter—there is a fundamental relation between the onset of plastic instabilities and the prescribed speed of deformation. Consequently, smooth flow as observed macroscopically may simply be a manifestation of a velocity mismatch between the internal processes, i.e., dislocation avalanches, and the applied rate. In the following, we present strong evidence derived from both experiments and simulations that this is the case.

Nb crystals with a nominal diameter of 2 μm and aspect ratio of 1:3 were cut from a ⟨110⟩-oriented Nb single crystal by focused ion beam (FIB) milling. The crystals were strained uniaxially in compression using a Hysitron TI-950 TriboIndenter equipped with a flat punch tip under displacement control [22]. Nominal displacement rates $\dot{u}$ varied between 0.06 and 30 000 nm/s, which translates into strain rates between 10^{-5} and $5\,s^{-1}$. All crystals were deformed to a total plastic engineering strain of ∼20%. The displacement-time profiles of the straining experiments were analyzed to extract slip events and their associated velocity-time profiles. Three-dimensional (3D) discrete dislocation dynamics (DDD) simulations of crystals with ⟨001⟩ orientation and diameters of 0.5, 1.0, and 2.0 μm were carried out under strain control to complement the experimental study. An atomistically

*Corresponding author: rmaass@illinois.edu

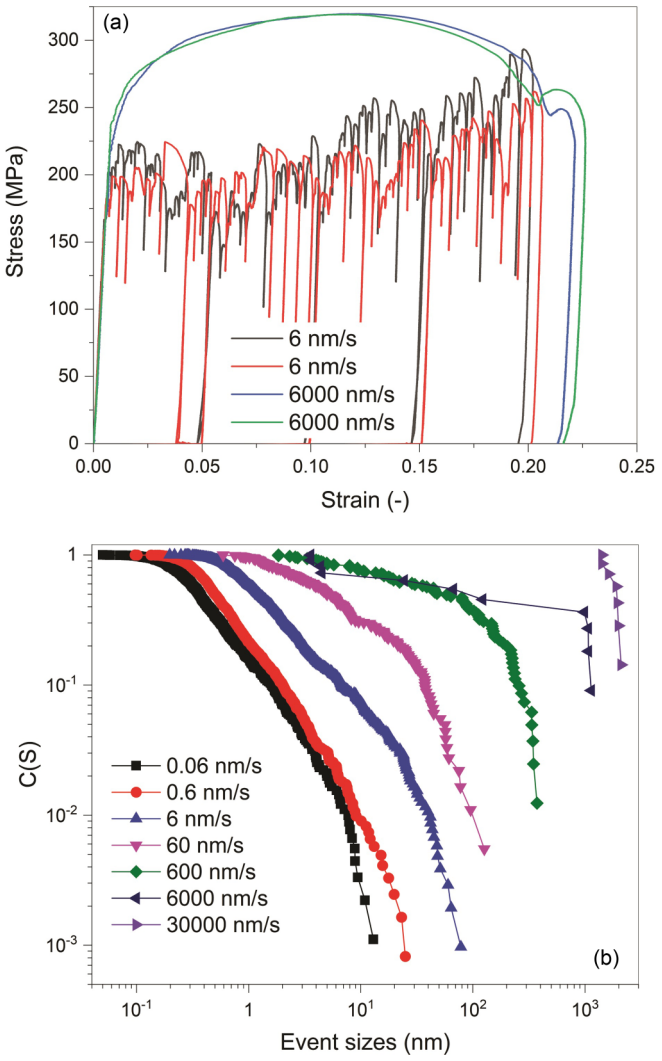

FIG. 1. (a) Engineering stress-strain curves for Nb⟨011⟩ crystals obtained at $\dot{u} = 6$ and $\dot{u} = 6000$ nm/s. (b) Stress-integrated complementary cumulative distribution, $C(S)$, for all tested rates.

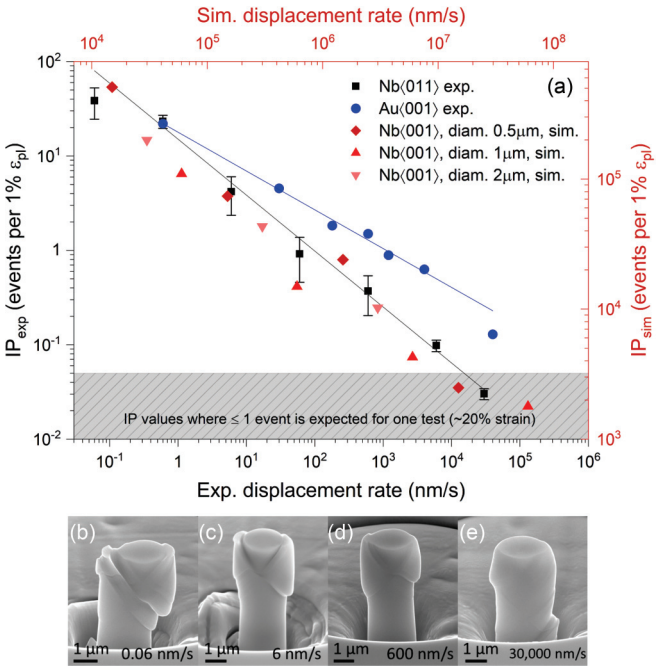

FIG. 2. (a) Intermittency parameter, IP, for Nb⟨011⟩ and Au⟨001⟩ obtained from experiments (left ordinate and lower abscissa) and for Nb⟨001⟩ obtained from DDD simulations (right ordinate and upper abscissa). (b)–(e) Scanning electron microscopy images for micron-sized Nb⟨011⟩ crystals deformed at $\dot{u} = 0.06,\ 6,\ 600$, and 30 000 nm/s.

informed mobility law for Nb is used. The applied strain rate ranged from 10 to 10^4 s^{-1} in the simulations (see Supplemental Material (SM) [27–30]).

Changing the applied displacement rate has a dramatic effect on the experimentally observed engineering stress-strain curves. Figure 1(a) compares two curves obtained for both 10^{-3} s^{-1} (6 nm/s) and 1 s^{-1} (6000 nm/s), respectively. Figure S1 displays curves obtained at all tested rates. Clearly, at higher applied rates, stress-strain instabilities cannot be detected and plastic flow appears smooth. It is worth noting that the strain-independent strain-rate sensitivity obtained for the micron-sized single crystals (~36 MPa/s) is in very good agreement with numbers known for bulk plasticity [31–33], with the only difference that the total stress scale of the small crystals is higher due to the expected size effect [34]. Analyzing the displacement jumps associated with the underlying instabilities allows constructing the stress-integrated complementary cumulative distribution [$C(S)$] for events detected at each applied displacement rate [Fig. 1(b)]. As known from previous works that have investigated avalanche size distributions, a truncated power law describes $C(S)$ well at lower applied rates. Increasing the rate gradually reduces the scaling due to an increasingly smaller fraction of small avalanches. This trend manifests itself due to merging of individual small avalanches and the fact that the corresponding velocity-size scaling is truncated at the low-velocity range. While the avalanche-size scaling exponent is not the focus of this study, $C(S)$ clearly shows how each experiment at the highest rate (seven tests in total) reduces the number of events per test to one. This means, even though there are no visible instabilities, a careful analysis of the displacement-time trace shows that the plastic flow rate of the micron-sized single crystals exceeds the applied rate by a factor of ~3–5: thus, the plastic stress-strain curve can be seen as one large continuous event.

The tendency for a decreasing number of intermittent events with increasing displacement rate is quantified in Fig. 2(a) (left ordinate and lower abscissa), showing a very consistent power-law relationship $IP = 15\dot{u}^{-0.59\pm0.02}$ between displacement rate and an intermittency parameter (IP) across more than five orders of magnitude for Nb. IP is defined as the number of slip events per 1% engineering strain. The error bars shown are 95% confidence intervals from the standard error of the mean, calculated based on the variation in IP across multiple sample tests (approx. 5 ~ 20 per drive rate). Given the maximum engineering strains of ~20%, the absence of intermittency in a single test ($IP < 0.05$) is expected for Nb when $\dot{u} > 16\,000$ nm/s, which is consistent with our observations. Figure 2(a) furthermore shows that a similar trend is obtained for the Au crystals (albeit with only one test

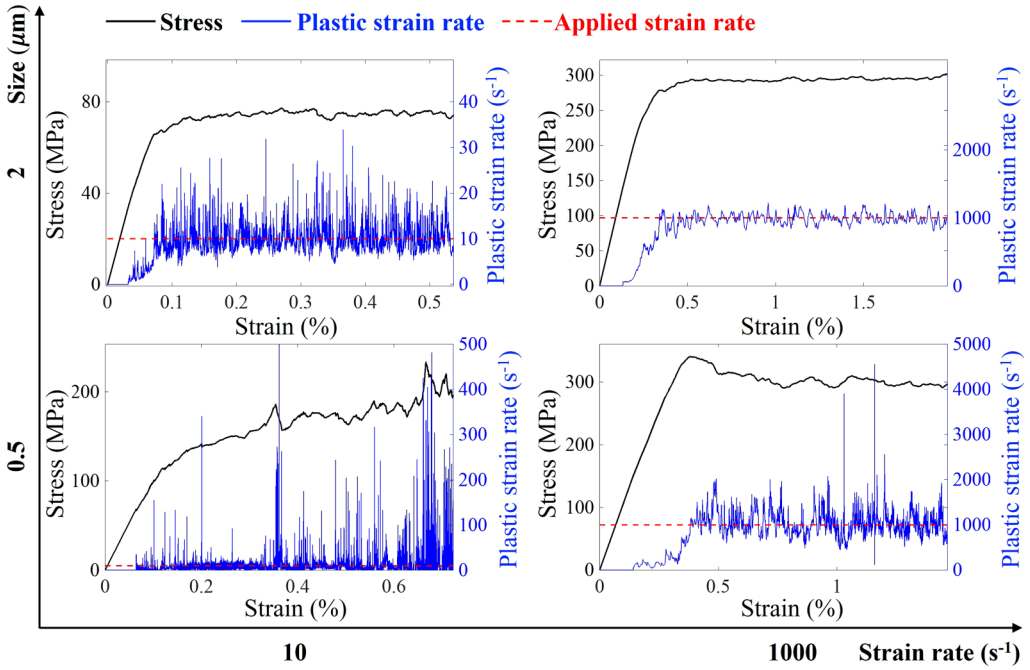

FIG. 3. Stress-strain curves obtained from DDD simulations for 2-μm and 500-nm large Nb⟨001⟩ crystals at 10 and 1000 s^{-1}. Right-hand y axis indicates the plastic strain rate and the horizontal dashed line is the applied strain rate.

per rate), with the difference that the data is shifted to the right and that $IP \propto \dot{u}^{-0.41\pm0.01}$. A shift to the right relative to the Nb can be understood with the fact that the slip velocity is ∼1 order of magnitude higher at any avalanche size and that the event size scales with velocity [18].

Along with the rate-dependent IP, clear variations in the deformation morphology were observed after testing. Figures 2(b)–2(e) compare the slip-line morphology between four different rates, evidencing that slip becomes increasingly delocalized with increasing rate. Analyzing the deformation morphology via computer-based image processing of scanning electron microscopy (SEM) micrographs allows determining the area fraction of the microcrystals that (within the resolution limit of the SEM micrographs) show visible slip traces, i.e., have undergone plastic shape changes. This quantification reveals how larger area fractions of deformation are obtained with increasing $\dot{u}$. The detailed results of this analysis are summarized in Table S1 in the SM [27]. In relation to Fig. 1(b), this suggests that discrete events recorded in the displacement-time signal must be composed out of numerous contributions from various locations within the crystal at higher rates. Thus, even though the event-size statistics suggests that larger rates result in fewer but larger avalanches, Figs. 2(b)–2(e) show that this must be a result of merging events throughout the crystal: plastic flow delocalizes. This can be rationalized by the fact that small differences in the resolved shear stress do not manifest themselves due to the high deformation rate, and, consequently, variability in the microstructure matters less.

In order to shed more light onto the underlying dislocation mechanisms as a function of applied rate and to scrutinize the hypothesis that a loss of intermittency is a fundamental consequence of a rate mismatch between collective dislocation events and the applied deformation rate, we conducted 3D DDD simulations on Nb⟨001⟩ micron-sized single crystals with the same height-to-diameter ratio. Some obtained stress-strain curves, together with the evolution of the plastic strain rate, are given in Fig. 3. The applied strain rate is considered as a threshold; if the magnitude of the continuous plastic strain rate in the time series is greater than the threshold, a dislocation avalanche is detected. As with the experimental data, an intermittency parameter is calculated and shown in Fig. 2(a) (right ordinate and upper abscissa). Their values are numerically higher than derived from the experimental results. This is due to numerous instrumental and method-specific factors, as we outline in detail in the SM [27]. Two dominating factors are (i) the difficulty of reaching pure strain control in experiments due to the finite machine stiffness effect [25] and (ii) the significantly different event resolutions. The effect of reducing the data sampling by a factor of 10 in the simulations is shown in the SM [27] in Fig. S3 and results in approximately 1 order of magnitude lower IP without any change of the observed scaling seen in Fig. 2(a). Despite the numerically different IP values, the power-law relation between IP and displacement rate is very well reproduced for all the considered sample sizes, as shown in Fig. 2(a). Remarkably, the power-law exponent is found to be −0.5, which is close to the experimentally determined value −0.59. This implies that $IP \propto \dot{u}^{-\alpha}$ holds for a wider strain-rate range and that this scaling is insensitive to the event resolution and the crystal sizes.

Moreover, Fig. 3 clearly demonstrates that with the increase of the strain rate and the external size, the plastic strain-rate evolution changes from crackling-noise type to quasiperiodic type. Concomitantly, the ratio between the fluctuation of the plastic strain rate and the applied strain rate becomes smaller. We note that Fig. 3 demonstrates how fluctuations are more pronounced in the smaller crystal (500 nm) at 1000 s^{-1}

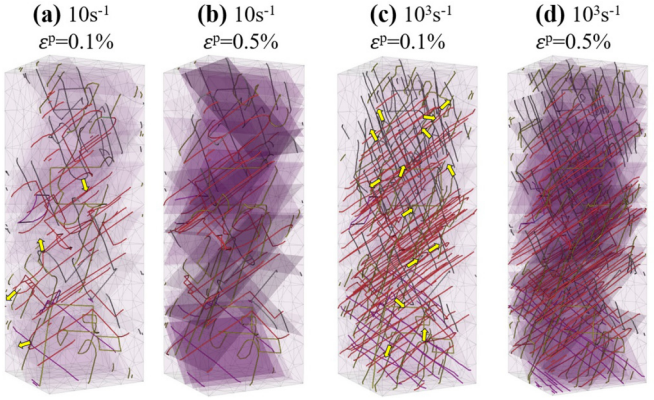

FIG. 4. (a)–(d) Microstructures at some specific plastic strains ε^p as indicated. Solid lines in different colors represent dislocations with different Burgers vectors. The darkness of the purple shaded regions is proportional to the local plastic strain. The yellow arrows in (a) and (c) indicate the bowing direction of dislocation sources.

than in the larger crystal (2 μm), which is a consequence of the fact that an equivalent strain rate is effectively a lower applied displacement rate for the 500-nm crystal. Thus, the velocity mismatch between slip in the smaller crystal and the applied rate is larger than for the 2-μm crystal, naturally leading to increased intermittency.

Through an in-depth examination of the microstructural evolution, it is found that at low strain rates, the operation of a few dislocation sources may contribute to one burst event. If these dislocation sources further trigger the correlated operation of several other dislocation sources, a sudden large ratio between plastic strain rate over applied strain rate is observed, which is the manifestation of a dislocation avalanche (slip event). Therefore, the burst behavior at low rate is controlled by the intermittent operation of small numbers of dislocation sources, leading to appreciable scatter. However, a strain burst in the high-strain-rate case requires the correlated operation of multiple dislocation sources in order to admit a plastic strain rate that is comparable to the high applied strain rate. Thus, the higher the applied rate, the more sources are active simultaneously, which effectively leads to a spatial merging of source activity and reduction of the discrete flow character. To keep up with high applied rates, dislocations quickly multiply to generate more sources at the early stage of plastic deformation, after which the dislocation density maintains a relatively stable value. One example of the larger dislocation density and larger number of operating sources at higher strain rate is given in Figs. 4(a) and 4(c) for a plastic strain of $\varepsilon_{pl} = 0.1\%$, where yellow arrows indicate the bowing direction of sources (edge and screw dislocations are indicated as solid lines of different colors). Due to the low screw dislocation mobility in bcc Nb, an increased density ratio between screw and edge dislocations is observed in comparison to the as-prepared sample. This ratio stabilizes after a short amount of anelastic strain to about 5–8 in the 2-μm crystals. This point is reached when the plastic strain-rate evolution curve in Fig. 3 attains the plateau around the applied strain rate. While both the dynamics of edge and screw dislocations contribute to individual bursts [35], recent simulations on W microcrystals reveal how the time-resolved evolution is dominated by slow screw dislocations [36]. A similar conclusion was made on the basis of a detailed avalanche velocity-profile analysis of both Au and Nb microcrystals deformed in experiments, revealing how the velocity relaxation in Nb is significantly longer in duration in comparison to Au, as expressed by a reduced decay exponent of the governing shape function [18]. This extended velocity relaxation of an avalanche in bcc is attributed to the fact that edge components are known to quickly exit the sample surface, whereas the screw components move much more slowly and also accumulate on their glide plane [37].

Further, our simulations can reveal the spatial distribution of plastic strain, which Fig. 4 indicates by shaded planes that are located on slip planes. The degree of darkness of the shaded planes indicates how much local plastic strain each slip plane has admitted. Consequently, darker shaded slip planes are seen at higher plastic strains for a given rate. More important is the observation that the number of active slip planes increases with increasing rate at a given plastic stain. This is easily seen when comparing Figs. 4(b) and 4(d), revealing how the localization of plastic flow decreases with increasing deformation rate. At high rates, a larger number of slip planes are activated and contribute to the relief of internal stresses built up in response to the high rate. These observations are in excellent agreement with the experimental observations in Fig. 2.

The observation of decreasing intermittency with increasing rate, and in particular the robust power-law scaling between IP and the applied rate in both the experiments (Nb⟨011⟩, Au⟨001⟩) and the simulations (Nb⟨001⟩), can be captured in a simple model and the DDD simulations. We consider the case of an idealized succession of elastic stress-strain regimes during which the stress rises followed by a drop in stress $\Delta\sigma$ due to an avalanche. Each elastic and plastic portion of the stress-strain curve is defined by its duration, Δt_1 and Δt_2, where the subscript 2 identifies the elastic part and 1 the plastic part (see Fig. S2). Under the assumption of a negligible overall strain hardening rate, which is well supported by Fig. 1(a), an equilibrium between the stress drop and the stress recovery during the elastic part can be equated as $\langle E(\dot{\varepsilon}_0 - \dot{\varepsilon}^p)\Delta t_1\rangle + \langle E\dot{\varepsilon}_0\Delta t_2\rangle = 0$, where E is the Young's modulus, the brackets indicate the average over all discrete events, and $\dot{\varepsilon}_0$ is the applied strain rate. Rearranging and defining $\dot{\varepsilon}^p = \rho b v$ and $\Delta t_1 = L/v$ allows expressing the burst frequency per unit strain as $IP = \frac{1}{\langle\dot{\varepsilon}_0(\Delta t_1+\Delta t_2)\rangle} = \frac{1}{\langle\dot{\varepsilon}^p\Delta t_1\rangle} = \frac{1}{\langle\rho\rangle bL}$, with b being the Burgers vector, ρ the dislocation density, v the dislocation velocity, and L the system size. We note that the equality is independent of material. The expression $IP \propto (\langle\rho\rangle bL)^{-1}$ can be further evaluated by interrogating the DDD simulations for a relationship between $\langle\rho\rangle L$ and $\dot{u}$. A power-law relationship between $\langle\rho\rangle L$ and $\dot{u}$ would not only support the above model, but also capture the fact that different crystal sizes are contained in the scaling displayed in Fig. 2(a). As shown in Fig. S3, both experimentally obtained exponents of $\alpha = 0.41$ and $\alpha = 0.59$ are in good agreement with the DDD data. This simple model implies that at higher applied deformation rates, a higher dislocation density (and thus a higher extent of correlated dislocation activity) is linked to the occurrence of avalanches.

The good agreement between experiments and simulations strongly support our initial hypothesis that smooth plastic flow of pure bulk single crystals may emerge as a result of an externally applied drive that has a higher velocity than the collective slip events admitted by the material. If this result can be generalized to the bulk scale, the occurrence of intermittent or smooth flow of pure single crystals would be another example of how the velocity of a microstructural process relates to the experimentally applied deformation rate, such as serrated and not-serrated flow in metallic glasses [6,38], or the PLC effect [3–5]. While we argue that there is strong evidence for this case, caution has to be used when generalizing to the bulk scale. It may appear straightforward to argue that strain-rate constancy naturally will lead to $\dot{u}$ exceeding the outer envelope of avalanche velocities, which for a 10-cm, large Nb⟨011⟩ bulk single-crystal specimen and $\dot{\varepsilon}_0 = 10^{-3}\,\mathrm{s}^{-1}$ ($\dot{u} = 100\,000$ nm/s) indeed would be the case. However, such an argument assumes that the slip dynamics is insensitive to the dramatic change in surface/volume ratio, and that net glide velocities are marginally affected by the changes in boundary conditions. This could be evaluated via bulk testing with the same displacement resolution as used here, which to our knowledge is experimentally not available. However, we note that selected evidence exists for the micro and bulk scale that crystal size does not affect the slip-size velocity [1,15,39]. Indeed, Becker and co-workers [1,39] have reported the velocity of suddenly deforming bulk Zn (hcp) and Al (fcc) crystals, where the slip rate is of the same order of magnitude as for the Au studied here.

In summary, we show that a transition from intermittent-to-smooth flow can be obtained for micron-sized Nb and Au single crystals via the increase of the applied deformation rate such that the latter is exceeding the velocity of the underlying dislocation avalanches (slip events). The reduction in intermittent response of the deforming crystals is captured in both experiments and simulations, and a simple power-law relationship between burst frequency and applied rate can be approximated to describe the reduction in burst frequency with increasing rate. Future experiments will show if the transition revealed here can be the fundamental origin of smooth bulk stress-strain behavior of pure single crystals.

G.S., Q.R., and R.M. thank P. M. Derlet, D. M. Dimiduk, K. A. Dahmen, and A. J. Beaudoin for fruitful discussions. This research was carried out in part at the Frederick Seitz Materials Research Laboratory Central Research Facilities, University of Illinois. R.M. is grateful for financial support by the NSF CAREER program (Grant No. NSF DMR 1654065) and for start-up funds provided by the Department of Materials Science and Engineering at UIUC. Y.C., G.C., and J.M. acknowledge support from the NSF through Grant No. DMR-1611342 and the US Department of Energy's Office of Fusion Energy Sciences, Project No. DESC0012774:0001.

[1] R. Becker and E. Orowan, Z. Angew. Phys. **79**, 566 (1932).
[2] R. F. Tinder and J. P. Trzil, Acta Metall. **21**, 975 (1973).
[3] P. G. McCormic, Acta Metall. **19**, 463 (1971).
[4] I. V. Shashkov, M. A. Lebyodkin, and T. A. Lebedkina, Acta Mater. **60**, 6842 (2012).
[5] A. Ziegenbein, P. Hähner, and H. Neuhäuser, Comput. Mater. Sci. **19**, 27 (2000).
[6] R. Maass and J. F. Löffler, Adv. Funct. Mater. **25**, 2353 (2015).
[7] T. Imanaka, K. Sano, and M. Shimizu, Cryst. Lattice Defects **4**, 57 (1973).
[8] R. M. Fisher and J. S. Lally, Can. J. Phys. **45**, 1147 (1967).
[9] M. C. Miguel, A. Vespignani, S. Zapperi, J. Weiss, and J. R. Grasso, Nature (London) **410**, 667 (2001).
[10] J. Weiss, T. Richeton, F. Louchet, F. Chmelik, P. Dobron, D. Entemeyer, M. Lebyodkin, T. Lebedkina, C. Fressengeas, and R. J. McDonald, Phys. Rev. B **76**, 224110 (2007).
[11] G. Ananthakrishna, S. J. Noronha, C. Fressengeas, and L. P. Kubin, Phys. Rev. E **60**, 5455 (1999).
[12] R. Maass and P. M. Derlet, Acta Mater. **143**, 338 (2018).
[13] D. M. Dimiduk, C. Woodward, R. LeSar, and M. D. Uchic, Science **312**, 1188 (2006).
[14] M. Zaiser, J. Schwerdtfeger, A. S. Schneider, C. P. Frick, B. G. Clark, P. A. Gruber, and E. Arzt, Philos. Mag. **88**, 3861 (2008).
[15] R. Maass, P. M. Derlet, and J. R. Greer, Small **11**, 341 (2015).
[16] N. Friedman, A. T. Jennings, G. Tsekenis, J.-Y. Kim, M. Tao, J. T. Uhl, J. R. Greer, and K. A. Dahmen, Phys. Rev. Lett. **109**, 095507 (2012).
[17] S. Papanikolaou, D. M. Dimiduk, W. Choi, J. P. Sethna, M. D. Uchic, C. F. Woodward, and S. Zapperi, Nature (London) **490**, 517 (2012).
[18] G. Sparks and R. Maass, Acta Mater. **152**, 86 (2018).
[19] G. Sparks and R. Maass, Phys. Rev. Mater. **2**, 120601(R) (2018).
[20] G. Sparks and R. Maass, Eur. Phys. J. B **92**, 15 (2019).
[21] D. M. Dimiduk, E. M. Nadgorny, C. Woodward, M. D. Uchic, and P. A. Shade, Philos. Mag. **90**, 3621 (2010).
[22] G. Sparks, P. S. Phani, U. Hangen, and R. Maass, Acta Mater. **122**, 109 (2017).
[23] Q. Rizzardi, G. Sparks, and R. Maass, JOM **70**, 1088 (2018).
[24] Y. Cui, G. Po, and N. Ghoniem, Phys. Rev. Lett. **117**, 155502 (2016).
[25] Y. Cui, G. Po, and N. Ghoniem, Phys. Rev. B **95**, 064103 (2017).
[26] X. Zhang, F. Shang, Y. Yu, Y. Yan, and S. Yan, Int. J. Solids Struct. **51**, 4519 (2014).
[27] See Supplemental Material at http://link.aps.org/supplemental/10.1103/PhysRevMaterials.3.080601 for further details on both the experiments and simulations.
[28] G. Po, Y. Cui, D. Rivera, D. Cereceda, T. D. Swinburne, J. Marian, and N. Ghoniem, Acta Mater. **119**, 123 (2016).
[29] G. Po, M. Lazar, D. Seif, and N. Ghoniem, J. Mech. Phys. Solids **68**, 161 (2014).
[30] R. Maass, M. Wraith, J. T. Uhl, J. R. Greer, and K. A. Dahmen, Phys. Rev. E **91**, 042403 (2015).
[31] S. Nemat-Nasser and W. Guo, J. Mater. Sci. Eng. A **284**, 202 (2000).

[32] T. E. Mitchell, R. A. Foxall, and P. B. Hirsch, Philos. Mag. **8**, 1895 (1963).
[33] T. L. Briggs and J. D. Campbell, Acta Metall. **20**, 711 (1972).
[34] J.-Y. Kim, D. Jang, and J. R. Greer, Scr. Mater. **61**, 300 (2009).
[35] M. Tang and J. Marian, Acta Mater. **70**, 123 (2014).
[36] Y. Cui, P. Po, P. Srivastava, K. Jiang, V. Gupta, and N. Ghoniem, Int. J. Plast. (2019), doi: 10.1016/j.ijplas.2019.08.008.
[37] D. Caillard, Acta Mater. **58**, 3493 (2010).
[38] R. Maass, D. Klaumünzer, and J. F. Löffler, Acta Mater. **59**, 3205 (2011).
[39] R. Becker and P. Haasen, Acta Metall. **1**, 325 (1953).